Optics & Laser Technology 88 (2017) 205–214

Contents lists available at ScienceDirect

Optics & Laser Technology

journal homepage: www.elsevier.com/locate/optlastec

Full length article

# Laser-assisted direct joining of AISI304 stainless steel with polycarbonate sheets: Thermal analysis, mechanical characterization, and bonds morphology

F. Lambiase[a,b,*], S. Genna[b]

[a] Dept. of Industrial and Information Engineering and Economics, University of L'Aquila, via G. Gronchi 18, Zona Industriale di Pile, 67100 (AQ), Italy
[b] CIRTIBS Research Centre, University of Naples Federico II, P.le Tecchio 80, 80125 Naples, Italy

ARTICLE INFO

*Keywords:*
Joining
Direct bonding
Bonding
Polymers
Diode
LAMP
AISI304
Polycarbonate
Hybrid joint
Morphology
Mechanical characterization
Direct joining

ABSTRACT

Laser-Assisted Metal and Plastic bonding (LAMP) of AISI304 sheets with polycarbonate sheets is investigated in this work. The process was performed by means of a high power diode laser with a maximum power of 200 W. The study introduces an integrated experimental approach aimed at understanding how the main process conditions (laser power and scanning speed) influence the direct-bonds quality, dimensions and presence of defects. To this end, the bonds dimension, shear strength, formation and dimension of bubbles in the bonded region were related to the temperature measurements and process parameters. According to the achieved results, the processing window that enables a good adhesion of the two materials is relatively small; this is due the activation of the adhesion phenomena that require overcoming an energy threshold. However, excessive energy levels reduce the bonds strength due to the increase in defects (bubbles) dimension that may combine (coalescence) leading to the formation of a central tunnel where the two substrates are completely detached.

## 1. Introduction

The employment of multi-material assemblies is becoming more and more attractive for transportation industries with the aim of reducing weight and fuel consumption owing to the possibility to exploit the materials characteristics. Thus, the joining technology represents a challenging issue since the materials being joined may show very different physical, thermal, and mechanical behaviors.

Conventional mechanical joining processes, such as riveting or bolted connections, usually involve a number of disadvantages including, stress concentration, long joining time owing to the requirement of hole-drilling and employment of external fasteners. To overcome these problems, a number of investigations have dealt with fast mechanical joining processes such as clinching for production of hybrid structures that involve different types of material including metals, polymers [1,2] and fibre reinforced polymers [3,4]. Although the most of the aforementioned problems can be solved by clinching, these connections can be performed on materials with ductile behavior [5] and involve stress concentration.

Despite of mechanical joining processes, adhesive bonding enables better distribution of stress during service life, good fatigue life, corrosion resistance, and high strength-to-weight ratio. However, this process is affected by a number of concerns including the requirement of specialized workers, substrate preparation and long curing time that increase the process cost, production time and produce high environmental impact [6]. Because of the increasing employment of hybrid structures, a number of investigations have been performed to overcome the above-mentioned problems and new processes have been developed. Thermo-mechanical processes such as Friction Lap Welding (FLW) [7–9], Friction Spot Welding [10], Friction Spot Joining [11], and Friction Based Stacking have been successfully employed to join polymers, reinforced polymers as well as hybrid structures comprising metal parts. However, the above-mentioned processes produce poor finishing surface in the weld region, involve high loads during the process thus requiring very stiff clamping systems.

In this context, Laser-based joining processes such as Laser Transmission Welding (LTW) and Laser-Assisted Metal and Plastic bonding (LAMP) enable to overcome almost all the above-mentioned limitations. LTW and LAMP offer several advantages over competitive joining processes: one step process, instantaneous bonding, highly localized heating, no vibration, low residual stresses [12] and flatness of the external surfaces, that improves the joint aesthetics. In addition,

* Correspondence to: Monteluco di Roio, 67040 (AQ), Italy.
*E-mail address:* francesco.lambiase@univaq.it (F. Lambiase).

http://dx.doi.org/10.1016/j.optlastec.2016.09.028
Received 20 June 2016; Received in revised form 7 September 2016; Accepted 14 September 2016

the laser heat is transferred directly in the joining zone at the components interface leading to very effective employment of energy.

LTW and LAMP exploit the optical transparency of some thermoplastics for a given laser wavelength. The laser beam passes through the transparent part (that is placed at the laser source side) and heats the absorbing underlying material. Then, the transparent part heats up and melts owing to heat conduction between the parts. The adhesion between the parts is thus achieved by pressing together the components during the laser scan [13]. As a result, physical or chemical bonding between the parts is achieved [14]; indeed, in the case of LTW of polymers a weld is produced, while in the case of LAMP the polymer adheres to the metal sheet forming a bond. Despite of adhesive bonding, LTW and LAMP enable different advantages including the requirement of a lower pre-cleaning of the surfaces [15], no curing time is needed, as the bond is ready as soon as the thermoplastic cools down. From a process point of view, LTW and LAMP offer higher degree of automation and higher standardization of the bond quality.

Typical processing parameters are power, scanning speed, stand-off-distance (that influences the laser beam dimension) and clamp pressure [16]. $CO_2$ laser sources are generally avoided (except for welding thin polymer films), since most plastics strongly absorb at $CO_2$ wavelength (10.6 μm). On the other hand, Nd:YAG laser and diode laser [17] are often employed for welding thicker sheets since high transparency of most of thermoplastics in the near infrared field.

So far LTW has been used to weld a wide range of thermoplastics including (PC), Polyamide (PA66), Polypropylene (PP), polyethylene (PE), Polymethylmethacrylate (PMMA), Acrylonitrile Butadiene Styrene (ABS), Polyethylene Terephthalate (PET) etc. [18–24]. On the other hand, LAMP has been adopted for producing different types of hybrid joints: PET-AISI304 [14], PET-titanium [25–29], PMMA-AISI304 [30,31], Polytetrafluoroethylene (PTFE) -titanium [32], PET-aluminum [33], ABS-zinc-coated steel [34] as well as for joining fibre reinforced thermoplastics (PC, PA66, PE) [18,35]. The transparency of the laser-sided material as well as the absorptivity of the underlying material are mandatory for the success of these processes. Thus, in LTW, in order to increase in absorption of the laser radiation and consequently the mechanical resistance of the weld, carbon black [36,37] either Carbon Nanotubes can be employed as described in [24]. On the other hand, when joining metals and polymers, surface pre-treatments such as those discussed in [38,39], UV–ozone or plasma pre-Treatment [40], anodizing of metal [33] or pre-oxidation of the metal surface [34] can be performed to improve the chemical bonding between the components. Bubbles formed near the joining interface have significant influence on the mechanical behavior of the bonds. Laser induced bubbles caused by the steep expansion induce the molten plastic to form an intimate contact with the metal substrate leading to strong mechanical anchoring effect as well as improved chemical bonding [29]. However, excessive bubble formation will degrade the shear strength because they reduce the bonded area and induce stress localization [33]. To study the influence of process parameters on development and size of the bubbles, the melting and vaporization curves of the polymer can be compared to temperature fields produced during laser-assisted bonding. However, because most of the polymers are not transparent to the IR, temperature analysis performed by means of infrared Cameras is not possible. Thus, the temperature profiles can be calculated by means of a Finite Element model that also enabled to estimate the melting and bubbles depth inside the polymer [31].

So far, different approaches have been followed to map the mechanical behavior of LTW welds and LAMP joints to the process conditions including: regression analysis [41–43], development of Artificial Neural Networks [44], optimization by Genetic Algorithms [25] as well as numerical analysis [23,45–49], which has been mainly employed to predict the temperature field in the joints [50,51]. Besides the optimization of the process parameters, to improve the mechanical behavior of such bonds, the control of bubble size can be performed by means of ultrasonic assisted LAMP [29], enabling an increase by four times of the shear strength of the bonds.

The main limit of most of the aforementioned papers is represented by treating specific aspects of the process; thus, in order to better understand how the process parameters influence the joints quality, dimension, presence of defects and temperature distribution, an integrated experimental approach is carried out here.

The bond produced by LAMP is characterized by a complex morphology that highly influences the mechanical behavior of the joint. The morphology of these joints depends on the temperature distribution, which influences the activation of the adhesion between the substrates, joint dimension, dimension of the bubbles in the joint seam, presence of other defects such as the “tunnel”.

To this end, experimental tests were performed on PolyCarbonate (PC) and a stainless steel AISI304. The influence of the main process parameters including the scanning speed and the laser beam power on the abovementioned aspects (temperature distribution, morphology, bubble formation and bonded region dimension and mechanical behavior of the bond) was analysed. Mechanical characterization of the joints was performed by conducting single lap shear tests.

**Table 1**
Mechanical properties of AISI304 and PC sheets.

| Material | Elastic modulus [GPa] | Ultimate tensile stress [MPa] | Elongation at rupture [%] |
|---|---|---|---|
| PC [52] | 2.7 | 65 | 110% |
| AISI304 | 197 | 535 | 65% |

## 2. Materials and methods

### 2.1. Materials

Extruded polycarbonate (PC) sheets 2.0 mm thick supplied by Bayer were bonded to rolled AISI304 sheets 1.0 mm thick. Polycarbonate is an amorphous thermoplastic employed in a wide range of applications owing to good optical transparency, relatively high tensile strength, and high toughness. AISI304 is a stainless steel characterized by high corrosion resistance and high toughness. The mechanical characteristic of both the materials are summarized in Table 1 and the thermal properties of PC sheets are reported in Table 2.

### 2.2. Laser-assisted direct-bonding setup

Laser–assisted bonds were made by means of a 200 W diode laser (DLR-200-AC, by IPG) with a fundamental wavelength of 975 nm. The laser radiation was transferred via an optical fibre, 6 m in length, to a collimator with recollimating lens, which produces a laser beam with 6 mm of diameter. The collimator was mounted on a 3+1 axis CNC system (finecut Y 340 M, by Rofin). Table 3 summarizes the detailed characteristics of the laser source.

During the laser direct-bonding experiments, the PC was placed at the laser beam side (being transparent to the laser beam), while the AISI304 sheet was placed at the opposite side. A clamping pressure of 1.0 MPa was applied to fasten the AISI304 and PC sheets during the laser assisted bonding process. A schematic representation of the laser assisted bonding setup and specimen is reported in Fig. 1. During the tests, the laser was switched on outside the sheets (with a distance of 10 mm from the sheets edge) in order to reach a steady state power and scanning speed before the entry region. Thus, the laser beam moved at the prescribed speed and produced the bonding (with a length of 20 mm). Finally, the laser beam proceeded outside the sheets to be switched off at a distance of 10 mm from the (opposite) edge. The overall bond length was 20 mm.

The main process parameters, i.e. the laser power (P) and scanning

**Table 2**
Thermal properties of PC sheets [53].

| Glass transition temperature [°C] | Crystalline melting temperature [°C] | Decomposition temperature [°C] |
|---|---|---|
| 145–150 | 215–230 | 377–462 |

**Table 3**
Laser source characteristics (IPG-DRL-200-AC).

| Characteristics | Symbol | Value | Unit |
|---|---|---|---|
| Emission centroid wavelength | λc | 975 ± 5 | [nm] |
| Emission linewidth | Δλ | 6 | [nm] |
| Nominal power | P | 200 | [W] |
| Modulation rate | | 50 | [kHz] |
| Output fibre core diameter | | 200 | [μm] |
| Collimated output beam diameter | | 6 | [mm] |
| Beam parameter product | BPP | 22 | [mm×mrad] |
| Cooling system | | air | – |

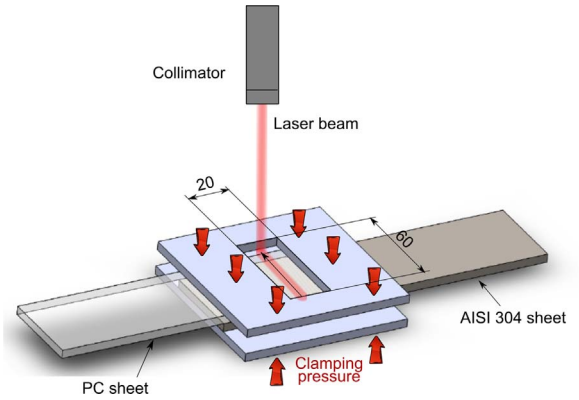


**Fig. 1.** Schematic representation of the laser assisted bonding setup.

speed ($S_S$), were varied according to a full 2×3 factorial experimental plan, whose levels are reported in Table 4.

### 2.3. Thermal analysis

To understand the influence of process parameters on temperature distribution, infrared analysis was performed on AISI304 sheets. These tests were performed without the PC, because the polycarbonate sheet is not transparent to the IR wavelength. It must be concerned that the temperature distributions measured during the effecting direct bonding process (with the PC overlaying the AISI304) are lower than those measured in the performed tests (without the PC) due to some differences, including reflection and absorption conditions, heat conduction towards the PC as well as variation heat capacity variation (mainly of the PC). Thus, these tests were not aimed at analysing the effective absolute temperature developing during the laser direct bonding of PC and AISI304, but rather to compare in a semi-quantitative way the temperature produced under different processing conditions. In addition, these tests were also performed to evaluate the suitability of these measurements as a technological test for indirect evaluation of bonds quality. Indeed, if this method yields reliable results, it can be used in conjunction with optimization methods to produce optimal temperature distributions, as reported in [54].

During these tests, an infrared (IR) camera A655SC by FLIR, equipped with a lens of 24.5 mm, was used. The IR camera was placed at a distance of 0.30 m from the specimen with an inclination α of almost 60°, as schematically reported in Fig. 2. According to the achieved setup, the AISI304 material showed an emissivity of 0.4. Such value was determined by comparing the infrared measurements with thermocouple signals recorded during heating tests performed on a precision heating table, model F20700080 by Velp Scientifica.

**Table 4**
Factorial plan: control factors and their levels.

| Control factor | Level 1 | Level 2 | Level 3 |
|---|---|---|---|
| Scanning Speed, Ss [mm/min] | 150 | – | 250 |
| Laser Power, P [W] | 100 | 150 | 200 |

### 2.4. Mechanical characterization of the bonds

Single lap shear tests were conducted to determine the mechanical characteristics of the bonds by using a Universal Test machine model 322.31 by MTS with a load capacity of 25 kN full-scale under quasi-static conditions (constant speed 0.2 mm/min) at room temperature. The geometry and specimen dimensions are reported in Fig. 3. Three replicates were performed for each bonding condition, then the average and standard deviation of the ultimate lap shear force $F_r$ were calculated.

### 2.5. Morphological characterization of the bonds

Optical analysis was performed before and after single lap shear tests to analyse the morphology of the bonds, measure the extension of the bonded area and observe the fracture of the specimens after single lap shear tests. To this end, a digital microscope (KH-8700 by Hirox) equipped by 2.11 Mega-pixel CCD Sensor was used. The MXG5040RZ lens was adopted, with a magnification of 50× and the Tiling tool was used to acquire the entire area. Once acquired the AISI304 and PC surfaces, the bonded area was measured by the Area tool. This allowed the evaluation of the shear strength of the bond.

## 3. Results and discussion

### 3.1. Temperature analysis

Fig. 4 depicts the typical thermography of a specimen, tested at P=100 W and $S_s$=150 mm/min, in three different phases when the laser beam is at the: (a) entry region, (b) central region and (c) exit region. The thermal analysis allowed understanding the variation and the distribution of temperature over the bonded and in the surrounding areas.

The temperature distribution along the scanning direction is highly uneven, as also shown in Fig. 5. Indeed, the distribution shows a saddle shape: the temperature at the entry and exit regions is higher than that reached in the center of the scanning path. A similar temperature distribution was also shown in other laser processes of AISI304 steel, such as laser forming [55]. This is due to the poor thermal conductivity of the material that does not allow fast heat dissipation from the edges (heat sink effect), as highlighted in Fig. 4.

The effect of the process parameters on the temperature distribution was studied more in detail to better understand the bond adhesion activation mechanism, formation of bubbles and other defects that may affect the bonds quality. Fig. 6 compares the temperatures along the bonding line (when the laser beam is at the exit region) with varying the scanning speed and laser power. Once again, it must be concerned that, these are only referral temperatures, since these tests were performed without the overlying polycarbonate.

As expected, the average and maximum values of temperature increased with decreasing the scanning speed (due to longer interaction time) and increasing the laser power, which led to the increase in the absorbed energy.

However, these curves are affected by the time factor; indeed, these curves are measured when the laser beam is over the exit region of the

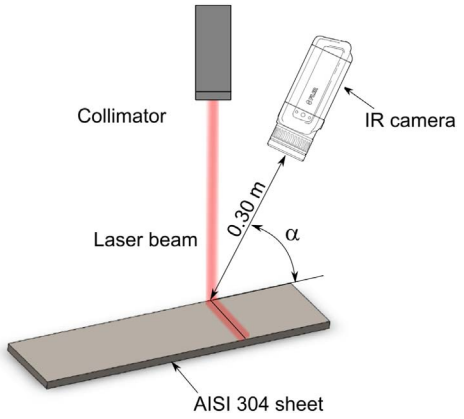


**Fig. 2.** Schematic representation of the IR setup.

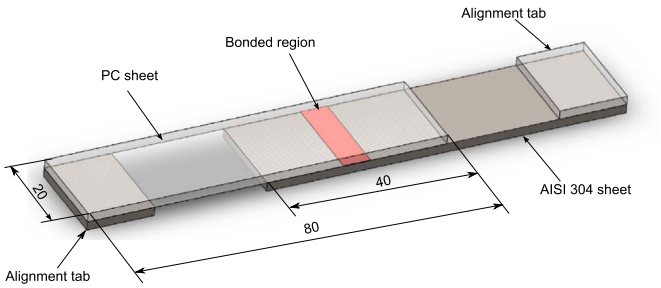


**Fig. 3.** Main dimensions and schematic of the specimens used for single lap shear tests.

sample. Thus, to better compare the temperature history of all the points lying on the beam axis path, the curve $T_{env}$, calculated as the envelop of the temperature histories of all these points (Fig. 7a), was adopted.

This was made almost automatically by means of the infrared camera post-processing software FLIR ResearchIR Max.

Thus, the variation of maximum temperature along the bonding line was obtained for all analysed processing conditions, as shown in Fig. 8 and the ratio of the maximum temperature (at the end point) $T_{max}$ to the temperature at the central region $T_c$ of the laser scan path was calculated.

Fig. 9 depicts the variation of $T_{max}$ and $T_c$ with varying the Line Energy (calculated as the ration of laser power to scanning speed). According to these results, $T_{max}$ increases more steeply than $T_c$ when higher values of LE are adopted, this means that more pronounced heat sink effect develops under processing conditions promoting high values of LE. This would produce detrimental effects on the bonds quality, because higher difference of temperature exist between the central and edge regions of the bonds.

### 3.2. Morphological analysis

The macrographs of the bonded regions achieved with varying the

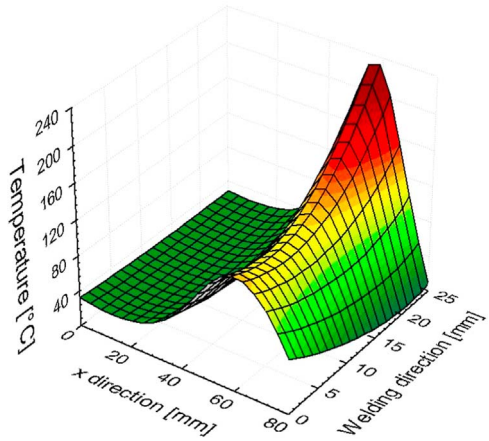


**Fig. 5.** Temperature distribution on AISI304 sheet after the exposure to the laser radiation (P=150 W; Ss=150 mm/min).

processing conditions are reported in Fig. 10. The bonded region is characterized by the presence of bubbles. Indeed, polycarbonate absorbs moisture at high rate. Thus, trapped moisture tends to form vapor above 120 °C and the vapor expansion creates bubbles in the sheet. The dimension of these bubbles is directly influenced by the temperature history during the laser-assisted bonding: indeed, larger bubbles are shown in correspondence of the laser seam, while the dimension of the bubbles reduces as moving towards the periphery, in agreement with the experimental findings reported in [25,26,56]. This is due to the higher temperature experienced in this region with respect to the surrounding ones. The bonded region geometry has an "hour-glass" shape: it is wider in correspondence of the entry and exit regions, while it is thinner in the central region. This is also due to the higher temperature reached during process in the edge regions, because of the above-mentioned "heat sink effect".

Fig. 11 depicts the upper view of the bond obtained at P=150 W, $S_s$=150 mm/s. Under this condition, which involves high energy input (LE=60 J/min), a tunnel region can be observed that develops in the exit region, likewise the observations reported in [31]. The presence of such a tunnel is detrimental because in this area there is no adhesion between the PC and the AISI304. The formation of the tunnel is due to the high vapor pressure that causes the detachment of the sheets and affects the effective bonded area. The tunnel region is more likely to appear in correspondence of the exit regions whereas higher temperatures were observed. However, when great input energy was used, the tunnel was shown all along the bonded area (e.g. P=200 W, $S_s$=150 mm/min, Fig. 10c).

The adoption of higher input energy (high laser power and/or low scanning speed), results in an increase in the temperature of the absorbing material (AISI304), with consequent higher heat conducted towards the overlying PC sheet. Thus, higher energy supplied results in the increase in the bonded area and average bond width, w (calculated as the ration of the bonded area by the bond length), as also reported in [20,26,57]. Under the minimum input energy condition (P=100 W,

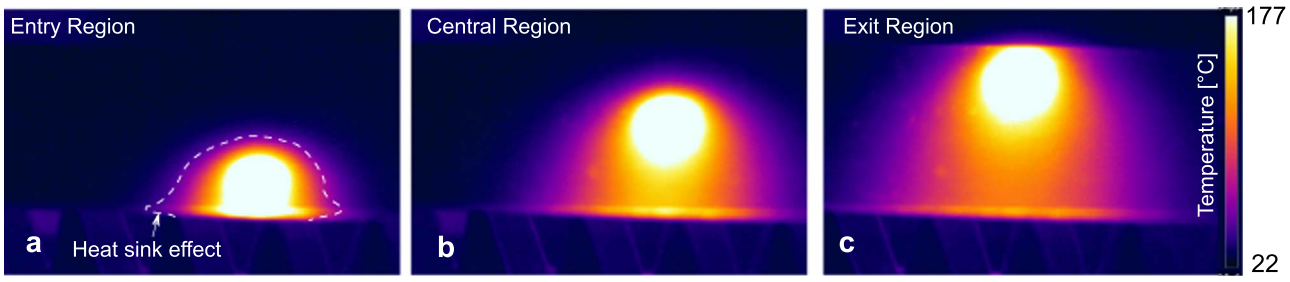


**Fig. 4.** Infrared analysis of the AISI304 sheet at the (a) entry region, (b) central region and (c) exit region. (P=100 W; Ss=150 mm/min).

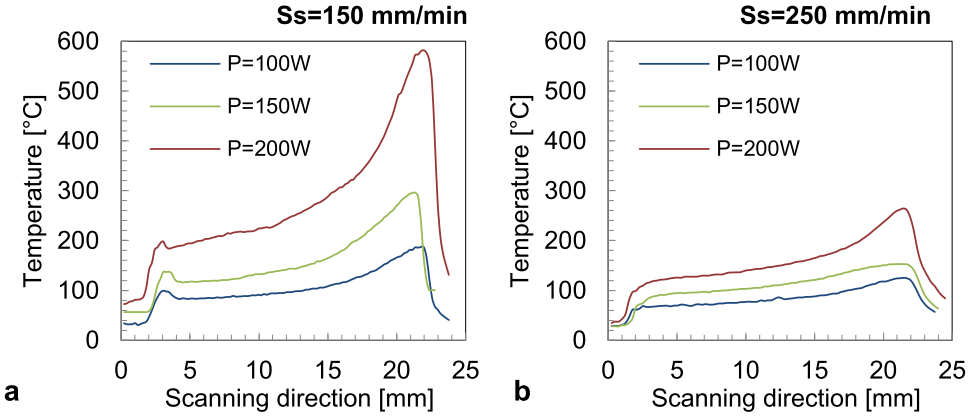


**Fig. 6.** Temperature distribution along the bonding direction on AISI304 sheet after the exposure to the laser radiation for different laser powers with scan speed equal to: (a) 150 mm/min; (b) 250 mm/min.

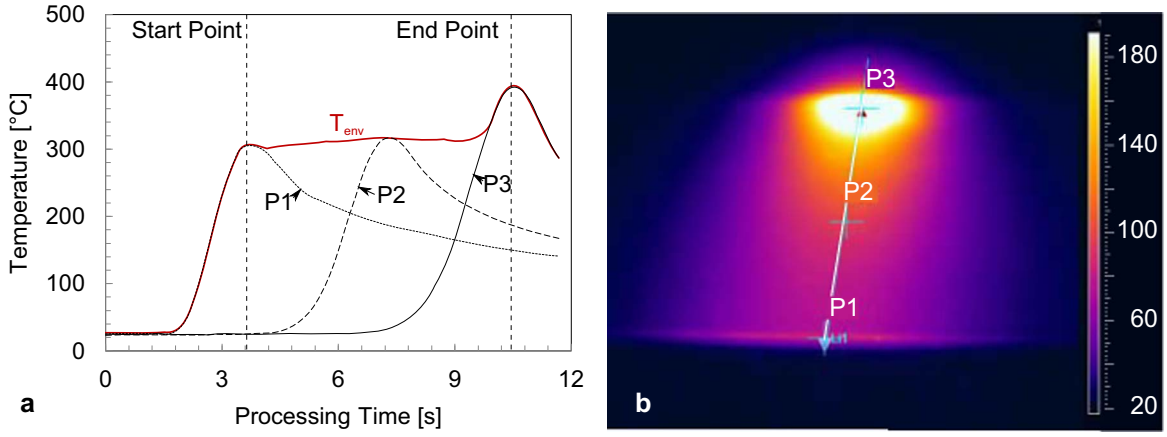


**Fig. 7.** Construction of curve $T_{env}$.

$S_s$=250 mm/min), the average bond width was smaller than the laser beam width $w_{beam}$. This processing condition produced a bond only at the entry and exit regions, as shown in Fig. 10d. On the other hand, all the other processing conditions produced a continuous bond with w > $w_{beam,}$ , as shown in Fig. 12. A similar trend was also reported in [25].

The macrographs of the central regions of the bonds were compared in Fig. 13a. As can be inferred, up to LE=40 J/mm, round bubbles can be clearly identified; however, as the line energy increases (from LE=48 J/mm) the coalescence of bubbles is shown with loss of circularity (especially in beam axis path). This yields to a dramatic reduction in the mechanical behavior of the bonds because in these areas the substrates are completely detached. In addition, the increase in the bubbles dimension either their coalescence reduces the effective bonded area and may facilitate the stress concentration leading to lower bonds performances. Thus, to determine the influence of the processing conditions on the bond quality, an analysis of brightness was performed as shown in Fig. 13b. Indeed, the bonded area appears brighter than the area of the bubbles, which are transparent and consequently appear darker (due to the color of the AISI304 substrate). As can be observed, for LE=24 J/mm the histogram is concentrated in the left part of the diagram, indicating the color distribution of the substrate (no bond was produced in the central region under this

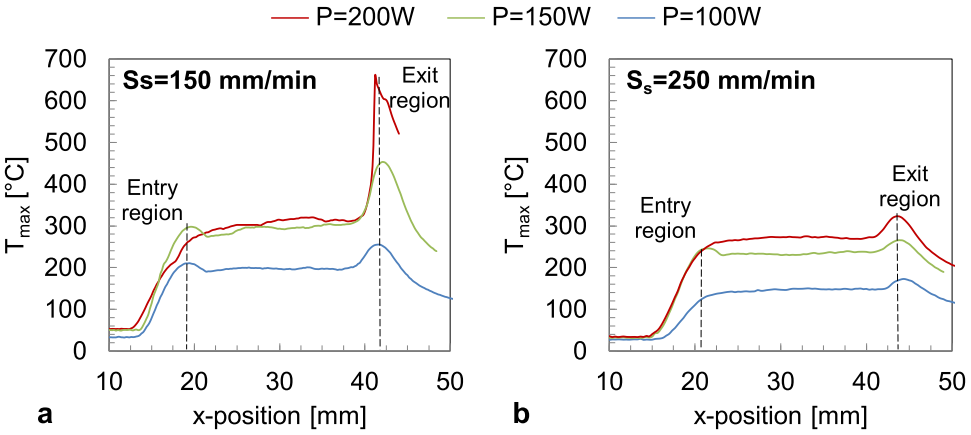


**Fig. 8.** Maximum temperature along the laser scan path on AISI304 sheet during the exposure to the laser radiation for different laser powers with scan speed of (a) 150 mm/min; (b) 250 mm/min.

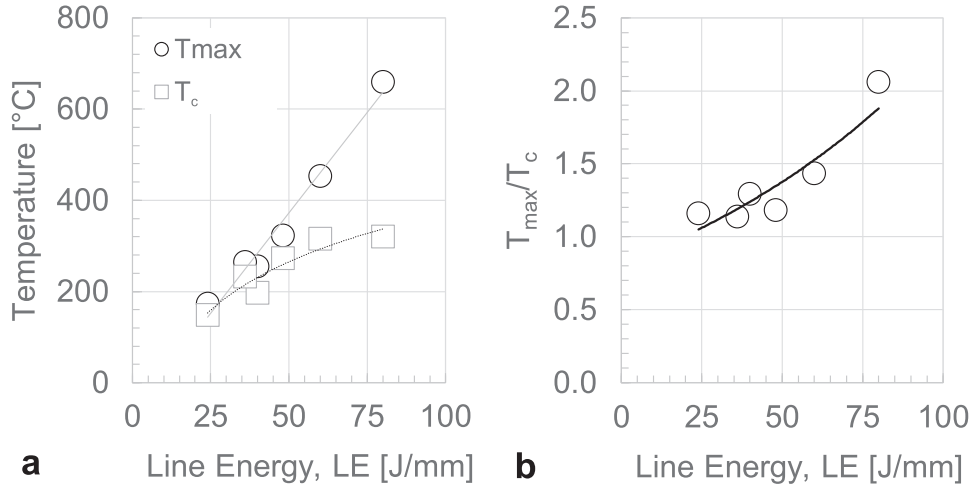


**Fig. 9.** Variation of temperature in the central and at the end of laser path with line energy.

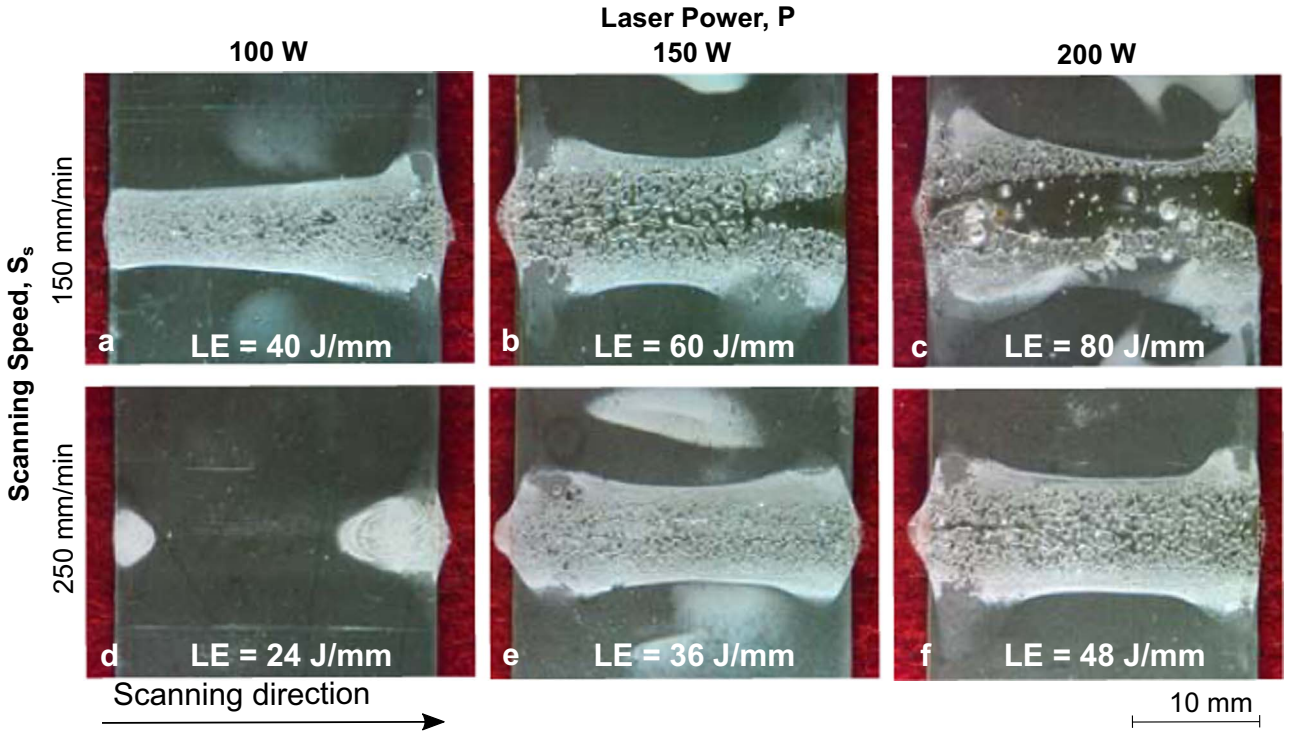


**Fig. 10.** Macrographs of the bonding regions of specimens with varying the processing conditions.

processing condition). For intermediate values of line energy LE=36 J/mm and 40 J/mm, the brightness histogram distribution is shifted towards the white color indicating a larger effective bonding area. On the other hand, higher values of LE=48 J/mm yield a flatter distribution due to the coalescence of the bubbles. Further increase in LE:LE=60 J/mm and LE=80 J/mm, resulted in evident shift of the histogram towards darker color (the color of the substrate) due to high coalescence effect that resulted in the formation of a large central tunnel.

For each distribution, the median color was calculated and reported as a function of the line energy, as reported in Fig. 14. The median color increases (indicating a larger bonded area) with LE up to LE=40 J/mm, then it decreases due to the excessive increase in the bubbles dimension, coalescence and tunnel formation.

### 3.3. Single lap shear tests

All the tested specimens failed by debonding of the substrates. This failure mode, which is similar to that occurring in adhesive bonding, is characterized by a catastrophic drop of the shear load after reaching a peak load.

Fig. 15a shows the variation of the ultimate lap shear force $F_r$ with the analysed process parameters. As can be inferred, the shear strength shows different trends with laser power when the two adopted scanning speeds were selected. Indeed, for $S_S$=150 mm/min, the shear strength $F_r$ shows a local minimum at the intermediate level of laser power P. This trend can be better understood by considering the variation of the morphology of the specimens, reported in Fig. 10. When the minimum level of P was selected, the bonded area was characterized by the presence of small bubbles. Increasing the laser power, resulted in a higher absorbed energy and consequently a larger bonded area. However, owing to the poor conductivity of the AISI304 material,

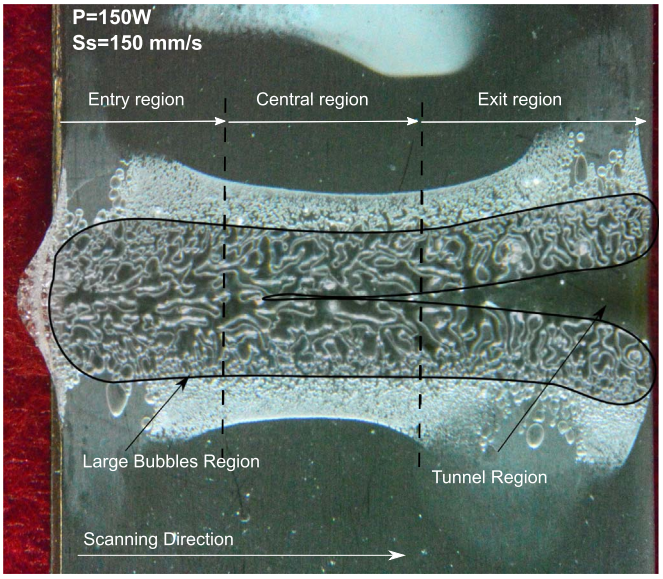


**Fig. 11.** Typical aspect of the joint: the bonding zones of specimens. (P=150 W, Ss=150 mm/s).

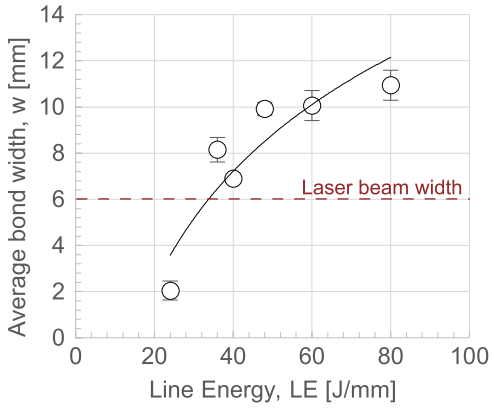


**Fig. 12.** Variation of average bond width with line energy.

great heat was stored inside the central region (−3 mm < y < 3 mm) leading to the formation of larger bubbles that reduced the shear strength of the bond. Furthermore, under such condition ($S_s$=150 mm/min, P=150 W) the formation of the tunnel in the exit region, which further affected the mechanical behavior of the bond, was observed. Further increase in laser power (P=200 W) resulted in a relative increase in shear strength. This was due to a better adhesion of the regions surrounding the scanned path, while the bonded area was characterized by a through tunnel that separated the AIS304 and PC substrates.

When the higher level of scanning speed was adopted ($S_s$=250 mm/min), a different trend of the ultimate lap shear force vs. laser power was observed. Actually, $F_r$ showed a local maximum at the intermediate level of P. For P=100 W the adhesion of the substrates was partially activated; this led to the development of a very weak behavior of the bonds. In addition, as can be also observed in Fig. 10, the parts were joined only at the extremities (where higher heat was stored), while it did not overcome the threshold value for the activation of the bonding development in the central region. When higher level of laser power was selected i.e. P=150 W, a steep increase in $F_r$ was observed in agreement with experimental findings reported in [42,57]. Indeed, the bonds produced under $S_s$=250 mm/min and P=150 W showed a regular shape and small bubbles all along the scanning path. However, further increase in laser power, i.e. P=200 W, produced excessive heat input that resulted in an increase in bubbles dimensions

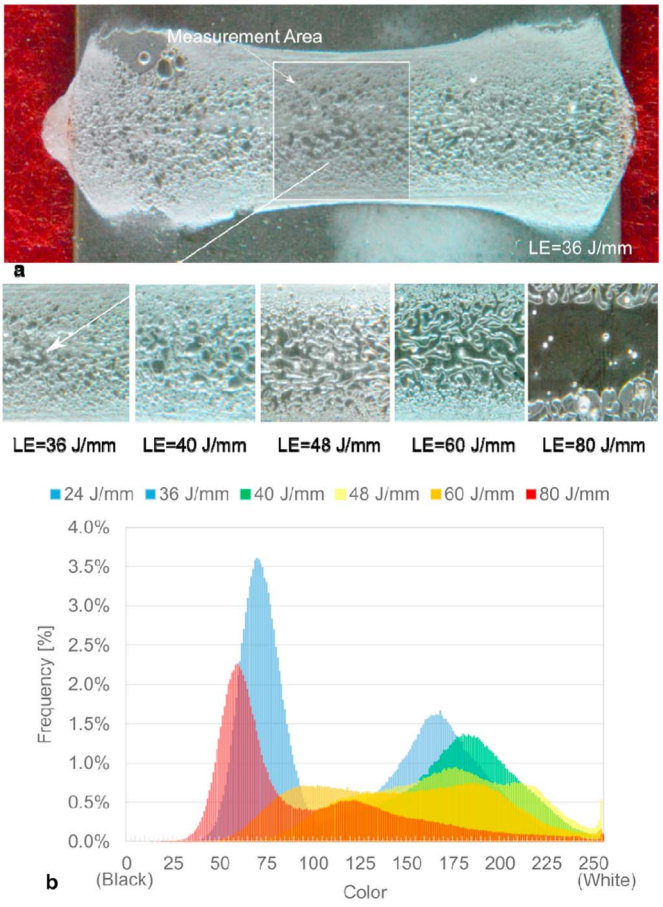


**Fig. 13.** Analysis of weld quality: (a) macrographs of the weld regions (b) histogram of brightness.

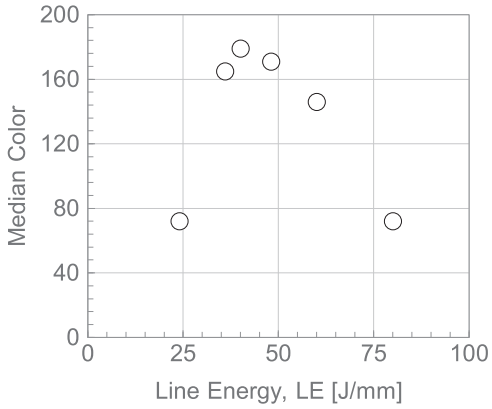


**Fig. 14.** Variation of the median color from brightness distributions with line energy.

and consequently a drop of the shear strength. In order to encompass with the laser power and scanning speed, the variation of the ultimate lap shear force with the Line Energy LE=P/$S_s$ was analysed, as reported in Fig. 15b. The minimum required Line Energy that allowed the formation of the bonds was LE=24 J/mm, under such conditions ($S_s$=250 mm/min, P=100 W), the bonding mechanism was activated at the extremities of the specimen. Increasing the line energy LE=36 J/mm produced a steep increase in shear strength that reached a local maximum. Further increase in LE up to LE=60 J/min resulted in a decrease in shear strength due to the development of larger bubbles in the bonded region while for LE=60 J/min ($S_s$=150 mm/min, P=150 W) it was caused by the development of the tunnel in the exit region. Further increase in line energy: LE=80 J/mm resulted in a

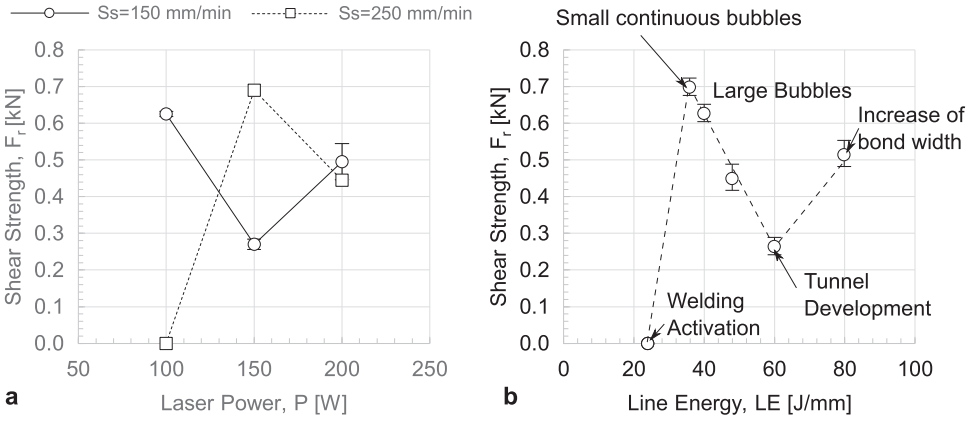


**Fig. 15.** Influence of the process parameters on the shear strength of the bonds and (b) variation of the shear strength Fr with the line energy.

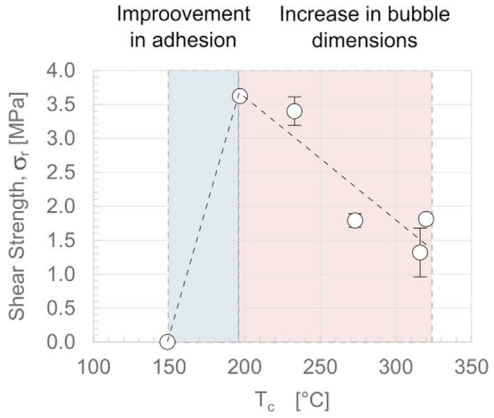


**Fig. 16.** Variation of the shear strength with average temperature of the AISI304.

slight increase in $F_r$ because of the development of small bubbles in the surrounding area. Below LE=60 J/mm, the trend of $F_r$ vs LE was similar to that reported in [24,42].

The shear strength $\sigma_r$ of the bonds, calculated as the ratio of $F_r$ to the bond area, was plotted against the average temperature measured by thermal analysis, as reported in Fig. 16. As can be inferred, the minimum temperature required to activate the bonding mechanism, is comprised between 150 °C and 200 °C. Then, the highest stress is achieved for T=200 °C and then reduces steeply. This is in agreement with the temperature characteristics of the polycarbonate due to the crystalline melting temperature ranges between 215 °C and 230 °C, as reported in [53]. Under the analysed process conditions, the maximum value of the average temperature of the AISI304 (and consequently that of the PC) was 320 °C that was lower than the degradation temperature of the polycarbonate [53].

### 3.4. Analysis of fracture surfaces

Fig. 17 depicts the fracture surfaces of polycarbonate sheets under relevant processing conditions: formation of tunnel defect (P=150 W; Ss=150 mm/s) and optimal processing condition (P=150 W; $S_s$=250 mm/min). As can be observed, the formation of the tunnel defect, shown in Fig. 17a–b produces a large area with a depth (measured in z direction) of almost 0.3 mm where the polycarbonate is completely separated from the AISI304. The bond develops only at the surrounding regions (characterized by a z-coordinate between 0.26 and 0.32 mm). On the other hand, under the optimal conditions, shown in Fig. 17c–d, the average depth is lower (because of lower energy was supplied during the laser-assisted bonding that led to lower formation of gas in the bonded area), and the tunnel defect is absent and smaller circular bubbles are present in the PC sheet.

Further investigation on the bonds quality was performed on the AISI304 sheets after single lap shear tests, as reported in Fig. 18. Under processing conditions being characterized by the minimum value of LE Fig. 18d, a small quantity of PC remains attached to the metal substrate. Increasing the LE resulted in an increase in the bonded area and consequently more PC material was found attached to the AISI304. This was due to the increase in temperature and consequently the adhesion between the substrates. However, the selection of process conditions involving high levels of LE resulted in a development and coalescence of larger bubbles that affected the mechanical performance of the bonds because this produced stress concentration, reduction in the bonded area and cross sectional area and presence of high quantity of gas that tended to separate the substrates [14].

## 4. Conclusions

An integrated experimental approach was followed to analyse the behavior of hybrid bonds performed on polycarbonate and AISI304 stainless steel made by Laser Assisted Metal and Polymer (LAMP) bonding. The process was performed by means of a high power diode laser with a maximum power of 200 W and maximum scanning speed of 250 mm/min. The main findings of the research are as follows:

- temperature analysis performed without the PC (conducted by means of infrared camera) was used to understand how the process parameters affect the temperature distribution and development of bond defects. Despite these measurements did not provide the exact values of temperature field developing during the laser-assisted bonding process, the employment of such measurements represents a viable way to determine a sound temperature window to optimize the shear strength of the bonds (200–230 °C). Thus, the employment of the Infrared Analysis performed on the solely metal represents an additional tool to design and optimize the laser-assisted bonding process;
- morphological analysis showed the main defects that can develop during LAMP process: increasing the value of Line Energy (LE) resulted in an increase in the bonded area, the dimension of bubbles, which are due to the expansion of gas at the PC/AISI304 interface, up to the coalescence of the bubbles with the formation of a central tunnel (called “tunnel defect”) where the substrates were completely detached.
- the analysis of the bonded area in the central region by means of the image analysis (brightness distribution) confirmed that the Line Energy had a marked effect on the dimension of bubbles, their coalescence and formation of the central tunnel, which are highly correlated with the strength of the bonds. In addition, this method can be potentially employed as a non-destructive tool to evaluate the

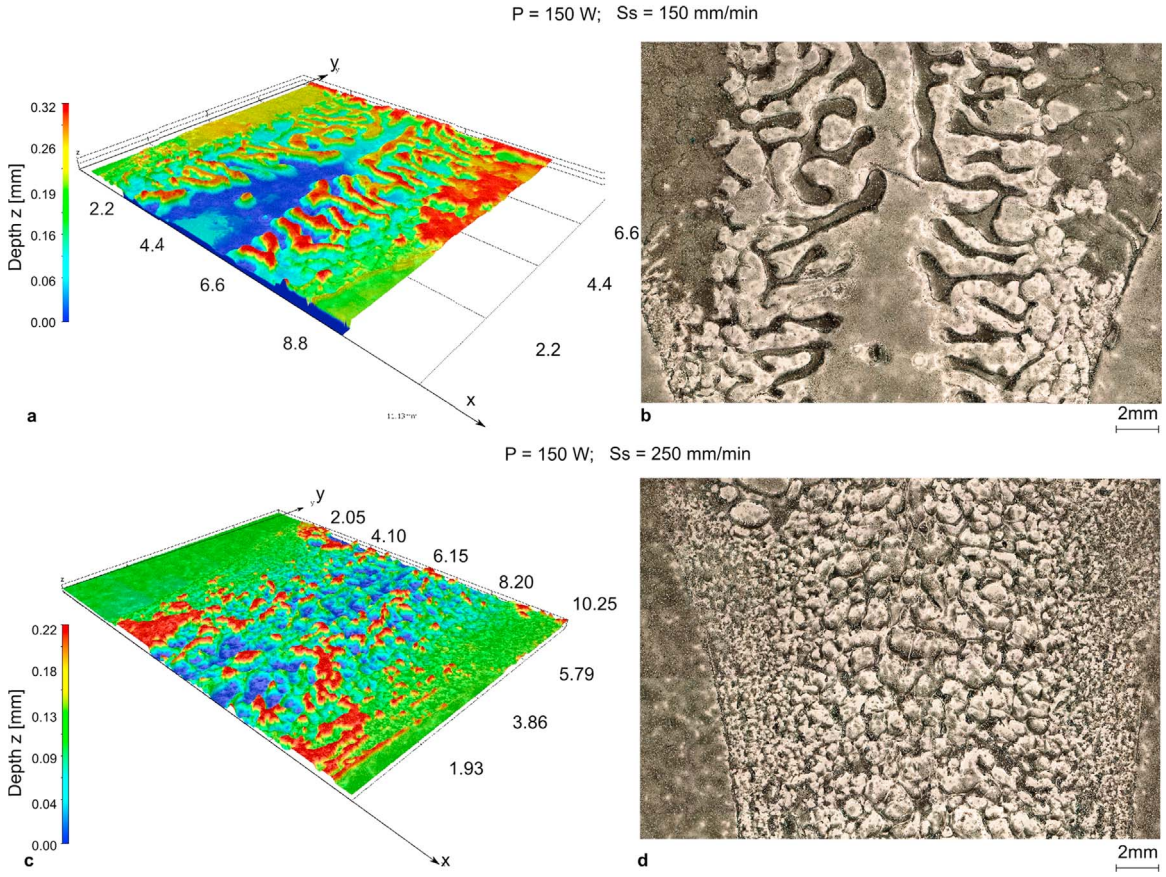


**Fig. 17.** Aspect of the PC sheet at the exit section after the single lap test; P=150 W: a), b) Ss=150 mm/min; c), d) Ss=250 mm/s.

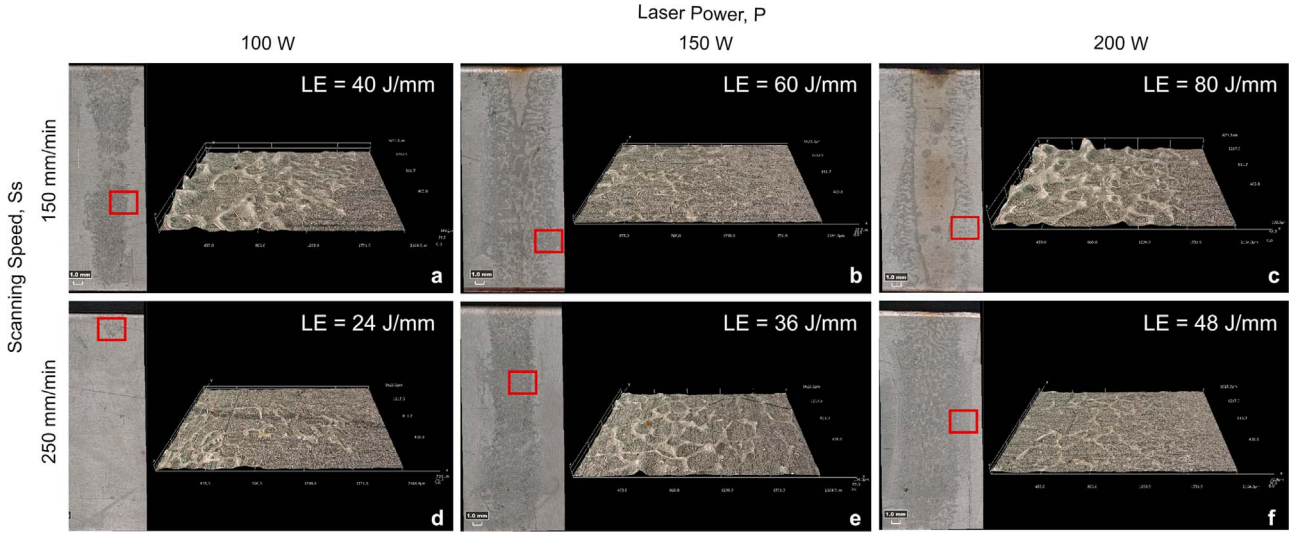


**Fig. 18.** Aspect of the AISI304 sheet after the single lap test; for each picture on the left the top view; on the right the 3d detailed.

effective bonded area for quality inspection purposes.

- optimal processing conditions developed for temperatures between 200 and 230 °C, which were produced by LE values between 36 and 40 J/mm. Under such conditions, the shear strength of the bonds reached 3.7 MPa being characterized by a low hourglass effect and small sized bubbles.

## Acknowledgments

The authors would like to thank Mr. G. Organtini (DIIIE - University of L'Aquila) to contribute during the setup and conduction of the experimental tests.

## References

[1] F. Lambiase, A. Di Ilio, Mechanical clinching of metal–polymer joints, J. Mater. Process. Technol. 215 (2015) 12–19.
[2] F. Lambiase, Mechanical behaviour of polymer-metal hybrid joints produced by clinching using different tools, Mater. Des. 87 (2015) 606–618.
[3] F. Lambiase, D.-C. Ko, Feasibility of mechanical clinching for joining aluminum AA6082-T6 and carbon fiber reinforced polymer sheets, Mater. Des. 107 (2016) 341–352.
[4] F. Lambiase, M. Durante, A.D. Ilio, Fast joining of aluminum sheets with glass fiber reinforced polymer (GFRP) by mechanical clinching, J. Mater. Process. Technol.

236 (2016) 241–251.
[5] F. Lambiase, Joinability of different thermoplastic polymers with aluminium AA6082 sheets by mechanical clinching, Int. J. Adv. Manuf. Technol. 80 (9–12) (2015) 1995–2006.
[6] C. Mandolfino, E. Lertora, S. Genna, C. Leone, C. Gambaro, Effect of laser and plasma surface cleaning on mechanical properties of adhesive bonded joints, Procedia CIRP 33 (2015) 458–463.
[7] K. Nagatsuka, S. Yoshida, A. Tsuchiya, K. Nakata, Direct joining of carbon-fiber–reinforced plastic to an aluminum alloy using friction lap joining, Compos. Part B: Eng. (2014).
[8] F.C. Liu, J. Liao, K. Nakata, Joining of metal to plastic using friction lap welding, Mater. Des. 54 (2014) 236–244.
[9] W.S. Junior, T. Emmler, C. Abetz, U.A. Handge, J.F. dos Santos, S.T. Amancio-Filho, V. Abetz, Friction spot welding of PMMA with PMMA/silica and PMMA/silica-g-PMMA nanocomposites functionalized via ATRP, Polymer 55 (20) (2014) 5146–5159.
[10] F. Yusof, M. Muhamad, R. Moshwan, M. Jamaludin, Y. Miyashita, Effect of surface states on joining mechanisms and mechanical properties of aluminum alloy (A5052) and Polyethylene Terephthalate (PET) by dissimilar friction spot welding, Metals 6 (5) (2016) 101.
[11] S.M. Goushegir, J.F. dos Santos, S.T. Amancio-Filho, Influence of process parameters on mechanical performance and bonding area of AA2024/carbon-fiber-reinforced poly(phenylene sulfide) friction spot single lap joints, Mater. Des. 83 (2015) 431–442.
[12] A. Yousefpour, M. Hojjati, J.-P. Immarigeon, Fusion bonding/welding of thermoplastic composites, J. Thermoplast. Compos. Mater. 17 (4) (2004) 303–341.
[13] V. Wippo, P. Jaeschke, M. Brueggmann, O. Suttmann, L. Overmeyer, Advanced laser transmission welding strategies for fibre reinforced thermoplastics, Phys. Procedia 56 (2014) 1191–1197.
[14] S. Katayama, Y. Kawahito, Laser direct joining of metal and plastic, Scr. Mater. 59 (12) (2008) 1247–1250.
[15] K.F. Tamrin, Y. Nukman, S.S. Zakariyah, Laser lap joining of dissimilar materials – a review of factors affecting joint strength, Mater. Manuf. Process. (2013) 130715070734009.
[16] E. Ghorbel, G. Casalino, S. Abed, Laser diode transmission welding of polypropylene: geometrical and microstructure characterisation of weld, Mater. Des. 30 (7) (2009) 2745–2751.
[17] A. Fortunato, G. Cuccolini, A. Ascari, L. Orazi, G. Campana, G. Tani, Hybrid metal-plastic joining by means of laser, Int. J. Mater. Form. 3 (S1) (2010) 1131–1134.
[18] X.F. Xu, P.J. Bates, G. Zak, Effect of glass fiber and crystallinity on light transmission during laser transmission welding of thermoplastics, Opt. Laser Technol. 69 (2015) 133–139.
[19] X.F. Xu, A. Parkinson, P.J. Bates, G. Zak, Effect of part thickness, glass fiber and crystallinity on light scattering during laser transmission welding of thermoplastics, Opt. Laser Technol. 75 (2015) 123–131.
[20] B. Acherjee, A.S. Kuar, S. Mitra, D. Misra, S. Acharyya, Experimental investigation on laser transmission welding of PMMA to ABS via response surface modeling, Opt. Laser Technol. 44 (5) (2012) 1372–1383.
[21] M. Chen, G. Zak, P.J. Bates, Description of transmitted energy during laser transmission welding of polymers, Weld. World 57 (2) (2012) 171–178.
[22] B. Acherjee, A.S. Kuar, S. Mitra, D. Misra, Application of grey-based Taguchi method for simultaneous optimization of multiple quality characteristics in laser transmission welding process of thermoplastics, Int. J. Adv. Manuf. Technol. 56 (9–12) (2011) 995–1006.
[23] B. Acherjee, A.S. Kuar, S. Mitra, D. Misra, Modeling and analysis of simultaneous laser transmission welding of polycarbonates using an FEM and RSM combined approach, Opt. Laser Technol. 44 (4) (2012) 995–1006.
[24] E. Rodríguez-Vidal, I. Quintana, C. Gadea, Laser transmission welding of ABS: Effect of CNTs concentration and process parameters on material integrity and weld formation, Opt. Laser Technol. 57 (2014) 194–201.
[25] X. Wang, H. Chen, H. Liu, P. Li, Z. Yan, C. Huang, Z. Zhao, Y. Gu, Simulation and optimization of continuous laser transmission welding between PET and titanium through FEM, RSM, GA and experiments, Opt. Lasers Eng. 51 (11) (2013) 1245–1254.
[26] H. Liu, K. Wang, P. Li, C. Zhang, D. Du, Y. Hu, X. Wang, Modeling and prediction of transmission laser bonding process between titanium coated glass and PET based on response surface methodology, Opt. Lasers Eng. 50 (3) (2012) 440–448.
[27] X. Wang, P. Li, Z. Xu, X. Song, H. Liu, Laser transmission joint between PET and titanium for biomedical application, J. Mater. Process. Technol. 210 (13) (2010) 1767–1771.
[28] C.-W. Chan, G.C. Smith, Fibre laser joining of highly dissimilar materials: commercially pure Ti and PET hybrid joint for medical device applications, Mater. Des. 103 (2016) 278–292.
[29] Y.J. Chen, T.M. Yue, Z.N. Guo, A new laser joining technology for direct-bonding of metals and plastics, Mater. Des. (2016).
[30] F.I. Hussein, E. Akman, B. Genc Oztoprak, M. Gunes, O. Gundogdu, E. Kacar, K.I. Hajim, A. Demir, Evaluation of PMMA joining to stainless steel 304 using pulsed Nd:YAG laser, Opt. Laser Technol. 49 (2013) 143–152.
[31] F.I. Hussein, K.N. Salloomi, E. Akman, K.I. Hajim, A. Demir, Finite element thermal analysis for PMMA/st.st.304 laser direct joining, Opt. Laser Technol. 87 (2017) 64–71.
[32] G.L. Georgiev, R.J. Baird, E.F. McCullen, G. Newaz, G. Auner, R. Patwa, H. Herfurth, Chemical bond formation during laser bonding of Teflon® FEP and titanium, Appl. Surf. Sci. 255 (15) (2009) 7078–7083.
[33] F. Yusof, M. Yukio, M. Yoshiharu, M.H. Abdul Shukor, Effect of anodizing on pulsed Nd:YAG laser joining of polyethylene terephthalate (PET) and aluminium alloy (A5052), Mater. Des. 37 (2012) 410–415.
[34] D.-J. Jung, J. Cheon, S.-J. Na, Effect of surface pre-oxidation on laser assisted joining of acrylonitrile butadiene styrene (ABS) and zinc-coated steel, Mater. Des. 99 (2016) 1–9.
[35] H. Liu, G. Chen, H. Jiang, D. Guo, Z. Yan, X. Wu, P. Li, X. Wang, Performance and mechanism of laser transmission joining between glass fiber-reinforced PA66 and PC, J. Appl. Polym. Sci. 133 (9) (2016) 1–8.
[36] B. Acherjee, A.S. Kuar, S. Mitra, D. Misra, Effect of carbon black on temperature field and weld profile during laser transmission welding of polymers: a FEM study, Opt. Laser Technol. 44 (3) (2012) 514–521.
[37] M. Aden, V. Mamuschkin, A. Olowinsky, Influence of carbon black and indium tin oxide absorber particles on laser transmission welding, Opt. Laser Technol. 69 (2015) 87–91.
[38] A. Heckert, M.F. Zaeh, Laser surface pre-treatment of aluminum for hybrid joints with glass fiber reinforced thermoplastics, J. Laser Appl. 27 (S2) (2015) S29005.
[39] H. Liu, H. Jiang, G. Chen, D. Guo, Z. Yan, P. Li, X. Wang, Investigation on the laser transmission weldability and mechanism of the graft-modified polyethylene and PA66, Int. J. Adv. Manuf. Technol. (2015).
[40] S. Arai, Y. Kawahito, S. Katayama, Effect of surface modification on laser direct joining of cyclic olefin polymer and stainless steel, Mater. Des. 59 (2014) 448–453.
[41] X. Wang, X. Song, M. Jiang, P. Li, Y. Hu, K. Wang, H. Liu, Modeling and optimization of laser transmission joining process between PET and 316L stainless steel using response surface methodology, Opt. Laser Technol. 44 (3) (2012) 656–663.
[42] B. Acherjee, D. Misra, D. Bose, K. Venkadeshwaran, Prediction of weld strength and seam width for laser transmission welding of thermoplastic using response surface methodology, Opt. Laser Technol. 41 (8) (2009) 956–967.
[43] B. Acherjee, A.S. Kuar, S. Mitra, D. Misra, Empirical modeling and multi-response optimization of laser transmission welding of polycarbonate to ABS, Lasers Manuf. Mater. Process. 2 (3) (2015) 103–123.
[44] B. Acherjee, S. Mondal, B. Tudu, D. Misra, Application of artificial neural network for predicting weld quality in laser transmission welding of thermoplastics, Appl. Soft Comput. 11 (2) (2011) 2548–2555.
[45] B. Acherjee, A.S. Kuar, S. Mitra, D. Misra, Modeling of laser transmission contour welding process using FEA and DoE, Opt. Laser Technol. 44 (5) (2012) 1281–1289.
[46] X. Wang, D. Guo, G. Chen, H. Jiang, D. Meng, Z. Yan, H. Liu, Thermal degradation of PA66 during laser transmission welding, Opt. Laser Technol. 83 (2016) 35–42.
[47] S.K. Sooriyapiragasam, C. Hopmann, Modeling of the heating process during the laser transmission welding of thermoplastics and calculation of the resulting stress distribution, Weld. World 60 (4) (2016) 777–791.
[48] P.J. Bates, T.B. Okoro, M. Chen, Thermal degradation of PC and PA6 during laser transmission welding, Weld. World 59 (3) (2014) 381–390.
[49] M. Aden, Influence of the laser-beam distribution on the seam dimensions for laser-transmission welding: a simulative approach, Lasers Manuf. Mater. Process. 3 (2) (2016) 100–110.
[50] T. Zoubeir, G. Elhem, Numerical study of laser diode transmission welding of a polypropylene mini-tank: Temperature field and residual stresses distribution, Polym. Test. 30 (1) (2011) 23–34.
[51] X. Wang, H. Chen, H. Liu, Investigation of the relationships of process parameters, molten pool geometry and shear strength in laser transmission welding of polyethylene terephthalate and polypropylene, Mater. Des. 55 (2014) 343–352.
[52] F. Lambiase, A. Paoletti, A. Di Ilio, Mechanical behaviour of friction stir spot welds of polycarbonate sheets, Int. J. Adv. Manuf. Technol. 80 (1) (2015) 301–314.
[53] C.L. Beyler, M.M. Hirschler, Thermal Decomposition of Polymers, SFPE, 3rd ed., Handbook of Fire Protection Engineering, One Batterymarch Park, Quincy, Massachusetts 02269, 2001, pp. 1–110.
[54] F. Lambiase, A.M. Di Ilio, A. Paoletti, Prediction of laser hardening by means of neural network, Procedia CIRP 12 (2013) 181–186.
[55] F. Lambiase, A. Ilio, A. Paoletti, An experimental investigation on passive water cooling in laser forming process, Int. J. Adv. Manuf. Technol. 64 (5–8) (2012) 829–840.
[56] X. Wang, C. Zhang, P. Li, K. Wang, Y. Hu, P. Zhang, H. Liu, Modeling and optimization of joint quality for laser transmission joint of thermoplastic using an artificial neural network and a genetic algorithm, Opt. Lasers Eng. 50 (11) (2012) 1522–1532.
[57] B. Acherjee, A.S. Kuar, S. Mitra, D. Misra, Laser transmission welding of polycarbonates: experiments, modeling, and sensitivity analysis, Int. J. Adv. Manuf. Technol. 78 (5–8) (2014) 853–861.